JOURNAL OF GEOPHYSICAL RESEARCH, VOL. 102, NO. B7, PAGES 14,835–14,852, JULY 10, 1997

Structure and sharpness of phase transitions and mantle discontinuities

Lars Stixrude

School of Earth and Atmospheric Sciences, Georgia Institute of Technology, Atlanta

Abstract. The structure of phase transitions expected from equilibrium thermodynamics is examined. We show that in binary systems, the shape of the coexistence region (phase loop) is controlled primarily by the partition coefficient K. We derive a general and simple one-parameter expression for the pressure dependence of the yield of the high-pressure phase and show that this function can be highly nonlinear: most of the transition occurs in a narrow interval near the boundary of the phase loop. Estimates of the effective width of binary phase transitions are less than half the total width of the coexistence region even for relatively mild partitioning ($K < 1/4$). We generalize these results to multiphase and multicomponent transitions. We show that the presence of nontransforming phases can affect the width of the transition substantially. We predict that the width of the olivine to wadsleyite transition in the presence of pyroxene and garnet is approximately half that of the binary phase loop at typical transition zone temperatures. The estimated effective width of this transition in the mantle (4-8 km) is marginally consistent with observations of high-frequency (0.5-1.0 Hz) P wave reflections from the 410 km discontinuity. We show that the effective width of the garnet to perovskite transition is sufficiently narrow to reflect S wave energy in the frequency range of ScS reverberations (10-40 mHz) and that this transition can account for the observed properties of the 710 km discontinuity.

Introduction

For some time, it has been widely accepted that solid-solid phase transitions are primarily responsible for the major seismic discontinuities in the Earth's mantle at 410 km and 660 km depth. This picture is supported by experimental observations that phase transitions from olivine to wadsleyite and spinel to perovskite plus magnesiowüstite, respectively, are known to occur in plausible mantle compositions at pressures that correspond to the depths of these discontinuities [*Jeanloz and Thompson*, 1983]. Experimental measurements of the acoustic velocities and equations of state of mantle minerals show that within present experimental uncertainties, changes in elastic properties associated with phase transitions agree well with those seismologically measured at 410 and 660 km depth for plausible mantle compositions [*Weidner*, 1985; *Duffy and Anderson*, 1989; *Ita and Stixrude*, 1992]. Moreover, experimental measurements of the temperature dependence of phase transition pressures (Clapeyron slopes) are consistent with seismological measurements of the topography of the 410 km and 660 km boundaries [*Revenaugh and Jordan*, 1991; *Vidale and Benz*, 1992; *Shearer*, 1991; *Wicks and Richards*, 1993].

A major discrepancy remains, however. The 410 km seismic discontinuity appears to be much too sharp (to occur over a depth interval too narrow) to be explained by the equilibrium olivine to wadsleyite phase transition. Experimental results indicate that the width of the phase transition is 8-19 km [*Katsura and Ito*, 1989; *Akaogi et al.*, 1989; *Fei et al.*, 1991], while seismological observations indicate a width of less than 4-6 km [*Leven*, 1985; *Benz and Vidale*, 1993]. The width of the transition from spinel to perovskite + magnesiowüstite is too small to resolve experimentally, but the 660 km discontinuity appears to be extremely sharp (1-4 km or 0.04-0.16 GPa) comparable to the precision of experimental measurements of pressure [*Richards*, 1972; *Lees et al.*, 1983; *Benz and Vidale*, 1993].

This issue is also important in the context of growing seismological evidence for the existence of other velocity discontinuities in the transition zone and lower mantle. One of the best characterized is the 520 km discontinuity [*Shearer*, 1991]. The origin of this feature is unknown, but since it appears to be nearly global in extent it is natural to assume that it is also caused by a phase transition. However, all the phase transitions which occur at the appropriate depths (wadsleyite to spinel, pyroxene to garnet, garnet to Ca-rich silicate perovskite + garnet) occur over substantial depth intervals (30-150

Paper number 97JB00550.
0148-0227/97/97JB-00550$09.00

km) and, except possibly for the wadsleyite to spinel transition, appear to be too broad to reflect significant seismic energy of the appropriate wavelengths. Though less well characterized, and possibly of only local extent, observations of seismic reflections and conversions from depths near 710, 900, and 1200 km also demand explanation [*Revenaugh and Jordan*, 1991; *Kawakatsu and Niu*, 1994]. Only one phase transition (from garnet to perovskite) is known to occur in this pressure regime in pyrolite-like compositions [*Irifune*, 1994]. This transition also occurs over a broad depth interval ($\approx$ 100 km).

The question which remains then is whether phase transitions alone, in an otherwise compositionally homogeneous mantle, can account for the existence and sharpness of seismic discontinuities. Essentially, three mechanisms have been proposed for reconciling the widths of phase transitions with those of seismic discontinuities. *Jeanloz and Thompson* [1983] explored the possibility that seismic discontinuities are caused by univariant phase transitions, transitions which occur suddenly, at a single pressure even in a multicomponent system.

The second mechanism envisions a compositionally stratified mantle in which the 660 km discontinuity represents a change not only of phase but also of composition [*Jeanloz and Thompson*, 1983; *Lees et al.*, 1983]. The change in composition is assumed to occur over a much narrower depth interval than the phase transition and to be primarily responsible for the sharpness of the discontinuity. *Bina and Kumazawa* [1993] have explored mechanisms by which the phase and compositional boundaries are thermodynamically coupled. These mechanisms require large chemical diffusivities which, in turn, may require substantial amounts of water or other fluxes in the deep mantle.

The third mechanism recognizes that phase transitions do not necessarily occur under equilibrium conditions in a dynamic system. *Solomatov and Stevenson* [1994] proposed that kinetic hindrances in a dynamic mantle may substantially decrease the width of the phase transitions.

Sharpness is essentially governed by the yield, or mole fraction, of the high-pressure phase as a function of pressure. The mechanisms discussed above have the effect of sharpening phase transitions by decreasing the total width over which the transition takes place. However, these mechanisms may not be required to explain the seismological observations. Equilibrium phase transitions in a homogeneous mantle can be effectively much sharper than the width of their corresponding phase loops suggest. In equilibrium, the yield of the high-pressure phase depends nonlinearly on pressure so that most of the phase transition may occur over a pressure interval much narrower than the total width.

The nonlinear dependence of yield on pressure has been overlooked in many previous seismic reflectivity studies, most of which assumed linear behavior, or a hyperbolic tangent function [*Richards*, 1972] that, as we show here, differs qualitatively from the expected form. The nonlinear dependence of yield on pressure for very broad transitions has been recognized previously by *Meijering and Rooymans* [1958] and in many experimental studies of mantle petrology [*Irifune and Ringwood*, 1987; *Irifune*, 1987, 1994], including that of *Akaogi and Akimoto* [1979], who emphasized nonlinearity as providing a possible mechanism for reflecting seismic energy from the broad pyroxene to garnet transition. *Helffrich and Bina* [1994] discussed the effect of the nonlinear shape of the olivine to wadsleyite transition as determined by specific solution models on seismic reflection from the 410 km discontinuity and recognized that the apparent width of a phase transition may be less than that of the phase transition interval.

A further effect which has been essentially overlooked is that the total width of a transition can be substantially reduced by the presence of other nontransforming phases. For example, as we show here, the presence of garnet and pyroxene substantially reduces the width of the olivine to wadsleyite transition. This is caused by the inherently multicomponent nature of the mantle and the equilibrium conditions of multiphase element partitioning. Nontransforming components in the mantle tend to act as buffers which reduce the compositional differences between coexisting low- and high-pressure phase assemblages and the width of the coexistence region.

Here, we reexamine the expected seismic velocity structure of equilibrium phase transitions and the extent to which they can explain the sharpness of seismic discontinuities. We show that the effective width of binary phase transitions can be substantially less than the width of the phase loop. In the ideal solution limit we derive an analytical expression for the yield of the high-pressure phase as a function of pressure which can be used in the analysis of experimental phase equilibrium data and seismic reflectivity modeling. The next section focuses on the important effects of nontransforming phases where we show that the width of binary phase transitions can be reduced substantially by the presence of other phases. Following sections generalize these results to multiphase and multicomponent transitions. Next, the effects of nonideality, nonisothermal conditions and the effective elastic properties of composites on the structure of transitions are examined and found to be generally small. Finally, the analysis is applied to understanding seismological observations of two discontinuities, the 410 km and the 710 km.

Binary Equilibria

Structure of Phase Transitions

Equilibrium between two binary solid solutions requires that the chemical potentials of the two components be equal in the coexisting phases. At pressure P and temperature T,

$$\mu_B^{\alpha}(P) - \mu_B^{\beta}(P) = 0 = RT \ln \frac{a_B^{\alpha}}{a_B^{\beta}} + \int_{P_B}^{P} \Delta V_B(P')dP' \quad (1)$$

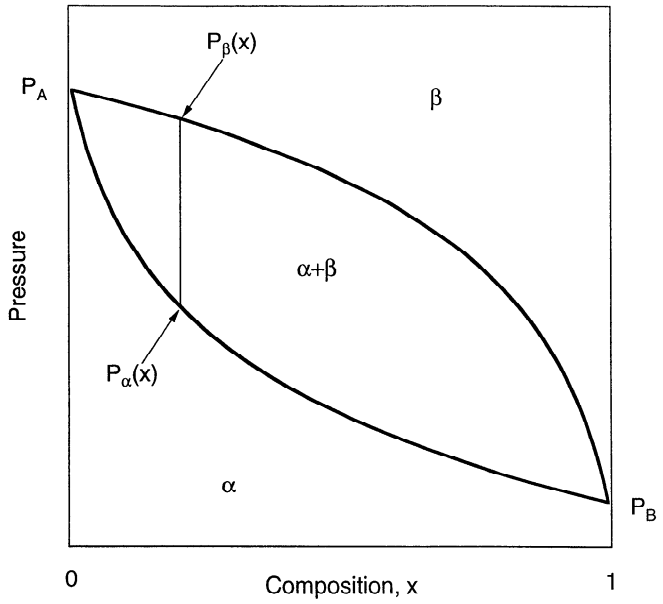

Figure 1. Notation used in the text. The stability fields of the low (α) and high (β) pressure phases are indicated as is the binary coexistence region (α+β). P_A and P_B are the transition pressures of the end-members. The width of the phase loop for a given bulk composition x is given by $P_\beta(x) - P_\alpha(x)$. The normalized pressure $P = (P - P_B)/\Delta P$, where $\Delta P = P_A - P_B$.

$$\mu_A^\alpha(P) - \mu_A^\beta(P) = 0 = RT \ln \frac{a_A^\alpha}{a_A^\beta} + \int_{P_A}^{P} \Delta V_A(P')dP' \quad (2)$$

where μ_i^j and a_i^j are the chemical potential and activity of component i in phase j, respectively, the P_i are the phase transition pressures in the end-member components, and the $\Delta V_i = V_i^\alpha - V_i^\beta$ are the volumes of transition. Figure 1 illustrates a binary coexistence region and some of the notation used in the discussion.

These equations are easily solved numerically for the mole fraction, or yield, of the high-pressure phase

$$f_\beta = \frac{(x - x_\alpha)}{(x_\beta - x_\alpha)} \quad (3)$$

for given bulk composition x if the relationship between activity and composition is known. Numerical results for particular solution models have been given before [*Lees et al.*, 1983; *Helffrich and Bina*, 1994; *Wood*, 1995]. Our purpose here, however, is to illustrate the general behavior of f_β and to derive an approximate analytical expression for use in the analysis of phase equilibrium and seismological data.

In the ideal solution limit the activity is uniquely defined [*Kerrick and Darken*, 1975]. Consider a binary substitutional solid solution with generalized chemical formula $(A_{1-x}B_x)_sZ_r$ that involves mixing on one type of atomic site. The solution has two components, A (formula A_sZ_r) and B (B_sZ_r). It is straightforward to derive the appropriate statistical mechanical partition function, and from this the ideal activity of component i (i=A, B) in phase j

$$a_i^j = \left(x_i^j\right)^s \quad (4)$$

where x_i^j is the mole fraction of component i in phase j. For nonideal solutions,

$$a_i^j = \left(\gamma_i^j x_i^j\right)^s \quad (5)$$

where γ_i^j, the activity coefficient is, in general, a function of composition, pressure and temperature.

We will assume (1) ideal solution theory, for which the activity coefficients are identically unity (γ_i^j=1 all i, j); strictly speaking, because the activity coefficients only appear in combination our analysis will also hold in the more general case $\gamma_A^\beta/\gamma_A^\alpha = \gamma_B^\beta/\gamma_B^\alpha = 1$; (2) that phase transitions in the mantle take place under essentially isothermal conditions, and (3) that the pressure interval over which phase transitions occur is small compared with the bulk modulus of the phases; this implies that we may neglect the pressure dependence of the ΔV_i over the range of integration. Assumptions 1 and 2 are relaxed and their effects examined in subsequent sections. The maximum error incurred by assumption 3 is readily found to be small and of the order $(P_A - P_B)/2B$, where B is the bulk modulus. Taking $B \approx 180$ GPa (the seismologically measured value at 410 km), we find that the fractional error is less than 3% even for wide transitions such as pyroxene to garnet ($P_A - P_B \approx 10$ GPa). Note that this approximation does not imply that the phases are incompressible. The ΔV_i appropriate to P and T must be used as these may differ substantially from the ambient pressure values.

We can derive an explicit one-parameter expression for the form of the phase loop and the yield in terms of the partition coefficient:

$$K \equiv \frac{x_\alpha(1 - x_\beta)}{x_\beta(1 - x_\alpha)} = \frac{x_B^\alpha x_A^\beta}{x_B^\beta x_A^\alpha} \quad (6)$$

where $x_j = x_B^j$ by recognizing that ΔV_A and ΔV_B are similar for most important mantle phase transitions. Writing $\Delta V_A/s = v - \delta v/2$ and $\Delta V_B/s = v + \delta v/2$, where v is the average volume of transition per solid solution species and δv is the difference between A and B components, the partition coefficient is found by combining (1), (2), and (6)

$$K = \exp\left[-\frac{\Delta P v}{RT}\left(1 + \frac{P - \bar{P}}{\Delta P}\frac{\delta v}{v}\right)\right] \quad (7)$$

where $\Delta P = P_A - P_B$ and $\bar{P} = (P_A + P_B)/2$. The partition coefficient is independent of pressure to lowest order in δv. The magnitude of the correction term is everywhere less than $\delta v/2v$ within the coexistence region, or less than 16% for phase transitions believed to occur in the mantle and, in most cases, including olivine to wadsleyite less than 5% (Table 1). Because the magnitude of the correction is less than typical relative uncertainties in $\ln K$, we make a final assumption 4 that δv=0 and that K can be approximated as being independent of pressure within the coexistence region.

Table 1. Comparison of End-member Volumes of Transition for Binary Phase Transformations of Geophysical Interest

Transition	A	B	s	ΔV_A	ΔV_B	$\delta v/2v$, %
ol=wa	Mg_2SiO_4	Fe_2SiO_4	2	1.62	1.53	-2.9
wa=sp	Mg_2SiO_4	Fe_2SiO_4	2	0.44	0.6	15.4
ol=sp	Mg_2SiO_4	Fe_2SiO_4	2	2.06	2.13	1.7
sp=pv+mw	Mg_2SiO_4	Fe_2SiO_4	2	1.97	2.14	4.1
sp=mw+st	Mg_2SiO_4	Fe_2SiO_4	2	7.2	7.88	4.5
2px=wa+st	$MgSiO_3$	$FeSiO_3$	1	4.07	4.35	3.3
2px=sp+st	$MgSiO_3$	$FeSiO_3$	1	4.5	4.95	4.8
sp+st=2il	$MgSiO_3$	$FeSiO_3$	1	0.48	1.17	41.8
il=pv	$MgSiO_3$	$FeSiO_3$	1	1.89	1.36	-16.3
mw+st=pv	$MgSiO_3$	$FeSiO_3$	1	0.8	0.77	-1.9
px=gt	$MgSiO_3$	$FeSiO_3$	1	2.79	3.54	11.8
px=gt	$Mg_4Si_4O_{12}$	$Mg_3Al_2Si_3O_{12}$	2	2.79	5.15	30.6
gt=pv	$MgSiO_3$	$FeSiO_3$	1	4.08	3.94	-1.7
gt=pv	$Mg_4Si_4O_{12}$	$Mg_3Al_2Si_3O_{12}$	2	8.16	6.92	-8.2

Zero-pressure volumes of transition for A and B end-member components (ΔV_A, ΔV_B) are shown along with the quantity $\delta v/2v$, equal to half their fractional difference. All volumes from *Jeanloz and Thompson* [1983], except those of $MgSiO_3$ and $FeSiO_3$ garnet and $Mg_3Al_2Si_3O_{12}$ perovskite [*Ita and Stixrude*, 1992] and $Mg_3Al_2Si_3O_{12}$ pyroxene [*Skinner and Boyd*, 1964]. Abbreviations are olivine (ol), wadsleyite (wa), spinel (sp), perovskite (pv), magnesiowüstite (mw), stishovite (st), orthopyroxene or clinopyroxene (px), ilmenite (il), garnet-majorite (gt). Note that where end-members are unobserved or unstable, fictive end-member volumes were used (e.g., Fe_2SiO_4 wadsleyite).

The form of the phase loop and the yield are found by rearranging (1):

$$\frac{x_\alpha}{x_\beta} = \exp\left(-\frac{(P-P_B)v}{RT}\right) = K^{\frac{P-P_B}{\Delta P}} \tag{8}$$

Combining this with a similar equation for $(1-x_\alpha)/(1-x_\beta)$ and defining the normalized pressure $\Pi = (P - P_B)/\Delta P$, the boundaries of the binary coexistence region are

$$x_\beta = \frac{1-K^{1-\Pi}}{1-K} \tag{9}$$

$$x_\alpha = \frac{K^\Pi - K}{1-K} \tag{10}$$

The definition of the normalized pressure is appropriate to the case depicted in Figure 1 where $P_B < P_A$. Since it is always possible to choose the B component to be the one with the lower transition pressure, this implies no loss of generality. This choice implies that the partition coefficient is such that $0 < K < 1$, a convention which we will retain throughout. The convention is not essential for the analysis and is assumed only for definiteness: it is worthwhile noting that the physical properties of the binary coexistence region depend only on $|\ln K|$, not on the value of K itself. The only effect of replacing K by $1/K$ is to relabel the phases such that β becomes the low-pressure phase.

The shape of the phase loop is governed by the value of K: smaller values (closer to zero) imply wider phase loops (Figure 2). The width of the phase loop is found from (9) and (10)

$$W(x) = P_\beta(x) - P_\alpha(x)$$

$$= \Delta P\left\{1 - \frac{\ln\left[K + x(1-x)(1-K)^2\right]}{\ln[K]}\right\} \tag{11}$$

which has the proper symmetry about x=0.5.

The yield of the high-pressure (β) phase for bulk composition x, as a function of pressure, is

$$f_\beta(\Pi) = \frac{x(1-K) - K^\Pi + K}{1 - K^{1-\Pi} - K^\Pi + K} \tag{12}$$

for $P_\alpha(x) < P < P_\beta(x)$. The dependence on pressure is sigmoidal and becomes increasingly nonlinear for smaller values of K (wider loops) (Figure 3).

The sense of inflection is opposite to that often assumed in seismic reflectivity modeling and numerical

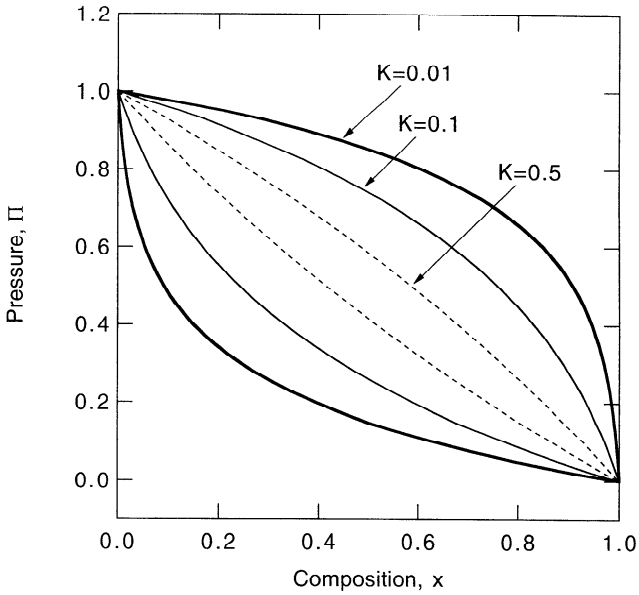

Figure 2. Binary coexistence regions for three values of the partition coefficient: K=0.01 (bold), K=0.1 (thin), K=0.5 (dashed).

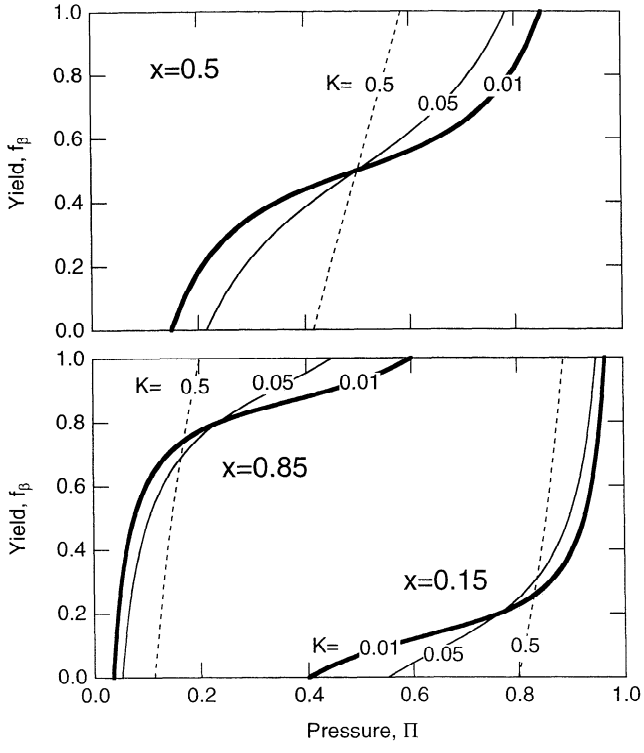

Figure 3. Yield of the high-pressure phase (f_β) versus normalized pressure for bulk composition (top) x=0.5 and (bottom) and x=0.15 and x=0.85. Results for three different values of the partition coefficient K are shown.

mantle convection studies. The yield f_β is commonly approximated by a hyperbolic tangent function which assumes that the transformation begins and ends gradually, with most of the transformation taking place near the middle of the loop [*Richards*, 1972; *Richter*, 1973]. In contrast, the expectation from equilibrium thermodynamics is that the region of rapid transformation lies at the most pressure-independent boundary of the phase loop. For small x the transformation ends rapidly, for large x it begins rapidly, and for x near 1/2 the beginning and end of the transformation are relatively abrupt.

Reflectivity and Effective Width

The nonlinear form (12) means that phase transitions can be effectively much sharper than the width of the corresponding phase loop would suggest. Most of the transition can occur over a pressure interval which is a small fraction of the total width of the loop.

This is important for understanding the seismic observability of mantle phase transitions. Because of its nonlinear shape, an equilibrium phase transition can reflect much higher-frequency energy than a first-order (linear) velocity discontinuity of the same width. To illustrate this, we have calculated the reflectivity as a function of frequency (wavelength) for equilibrium binary phase transitions [*Aki and Richards*, 1980]. We focus on near-normal incidence reflection because of its parametric simplicity: The reflection coefficient depends only on the appropriate (P, SV, SH) impedance contrast; the density and velocity jumps need not be specified separately [*Lees et al.*, 1983]. Moreover, near-normal incidence is a good approximation to the geometry of many of the relevant seismic observations: The incident angles of underside $P'P'$ reflections from the 410 km and 660 km discontinuities, for example, are sufficiently small ($i = 10^\circ - 20^\circ$) that the reflection coefficient should differ by less than 20% from the normal incidence value.

Figure 4 shows the reflection coefficient R of binary phase transitions for a range of partition coefficients that spans geophysically relevant values. We have found that the reflectivity of phase transitions can be usefully approximated by that of a linear transition with an effective width W_{eff} that is smaller than that of the phase transition (Figure 5). We take the effective width of a phase transition to be

$$W_{\text{eff}} = 1/f'_\beta(\Pi_\phi) \tag{13}$$

where $f'_\beta = (\partial f_\beta/\partial \Pi)$ and Π_ϕ is the pressure at which a specified fraction of the transition ϕ is complete:

$$\begin{aligned} f_\beta(\Pi_\phi) &= 1 - \phi \qquad x < 0.5 \\ f_\beta(\Pi_\phi) &= \phi \qquad x > 0.5 \end{aligned} \tag{14}$$

For $\phi = 1/3$, this measure of the effective width has a particularly simple seismological interpretation: a lin-

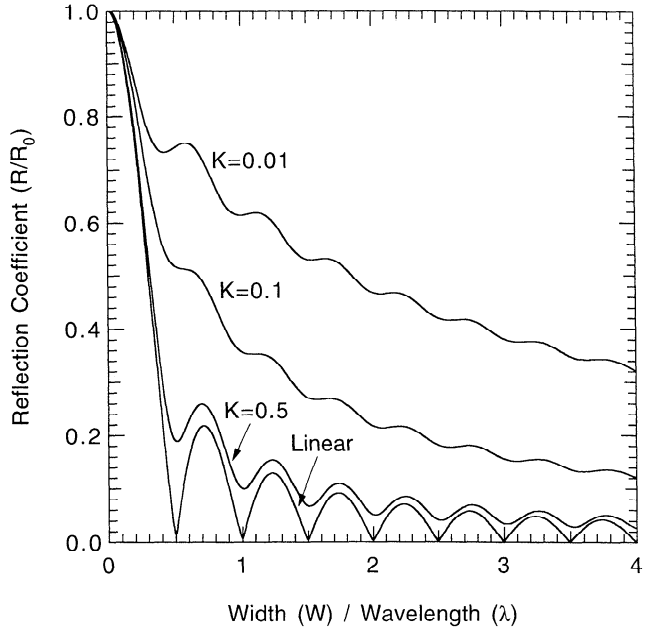

Figure 4. Reflectivity of equilibrium binary phase transitions calculated from (12) with $x = 0.1$ and various values of the partition coefficient K as a function of the width of the transition. The normal-incidence reflection coefficient is normalized to its zero frequency value and the width of the transition normalized to the seismic wavelength. The reflectivity of phase transitions is compared with that of a linear (second order) discontinuity.

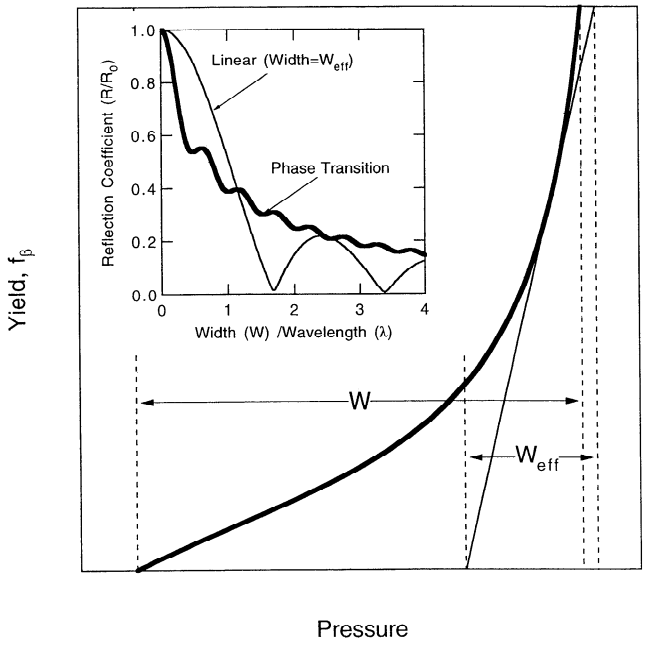

Figure 5. The form of a binary transition of width W is compared with its linear approximation with an effective width W_{eff}. The binary transition shown has $x = 0.15$ and $K = 0.01$. The linear approximation has the same slope as the equilibrium transition at $f_\beta = 2/3$. The inset shows that the phase transition and its linear approximation have similar normal-incidence reflectivity.

ear discontinuity of width W_{eff} is significantly reflective ($R/R_0 > 1/3$, where R_0 is the long-wavelength limiting value of R) over the same range of frequency as the phase transition. This relationship holds to within 10% in frequency over the entire range of geophysically important values of K (0.01 to 1) and x (0 to 0.2).

The effective width of a phase transition can be as little as 1/10 of the actual width for $K = 0.01$ (Figures 5 and 6). This means, for example, that phase transitions as wide as 40 km can reflect 1 Hz P wave energy. This is particularly important for understanding potential reflections from phase transitions with very strong partitioning, such as the pyroxene to garnet and garnet to perovskite transitions. For more moderate partitioning relevant to the olivine to wadsleyite transition ($K \approx 0.5$) the effect of nonlinearity is smaller. However, as we show in the next section, other effects are important for the olivine to wadsleyite transition, including the effect of nontransforming phases, which can also significantly increase high-frequency reflectivity.

Effect of Nontransforming Phases

This section focuses on the most important generalization of the binary case: phase transitions that take place in the presence of other nontransforming phases. All mantle phase transitions take place in the presence of nontransforming phases: pyroxene and garnet in the case of the olivine to wadsleyite transition. Moreover, nontransforming phases can have a large effect on the reflectivity of a phase transition by reducing the width over which it occurs. Because they are in equilibrium with the transforming phases, nontransforming phases affect the pressure dependence of the yield of the high-pressure assemblage and the structure of the resulting discontinuity. The origin of this effect is illustrated schematically in Figure 7.

The equations for the form of the phase loop and the yield of the high-pressure assemblage are derived in Appendix A. We consider a transition from a low-pressure phase $\alpha 1$ to a high-pressure phase $\beta 1$ in the presence of n nontransforming phases γi, $i = 1, n$. All phases are assumed to be ideal binary solid solutions with mixing on one type of atomic site. The bulk compositions of high- (x_β) and low- (x_α) pressure assemblages are

$$x_\alpha = \frac{K^\Pi - K}{1 - K}(1 - S_\gamma) \tag{15}$$

$$x_\beta = \frac{K^\Pi - K}{1 - K}[1 - S_\gamma - F_T(1 - K^{-\Pi})] \tag{16}$$

The yield of the high-pressure assemblage is

$$f_\beta(\Pi) = \frac{x(1 - K) - (K^\Pi - K)(1 - S_\gamma)}{F_T(1 - K^{1-\Pi} - K^\Pi + K)} \tag{17}$$

This expression properly reduces to (12) in the binary limit (F_T=1) for which the sum involving the composition of the nontransforming phases, S_γ (A6), vanishes.

In the applications section below, we use (17) to examine the structure of the olivine to wadsleyite transition. Here, we consider as an example the simple case, n=1, relevant to experimental studies of the Mg-rich portion of the MgO-FeO-SiO_2 system in which olivine

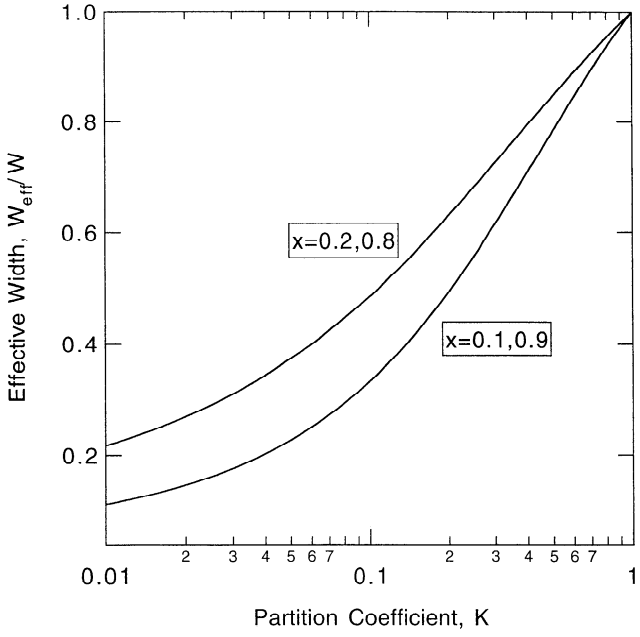

Figure 6. Ratio of the effective width, W_{eff}, to the total width of the phase transition for the geophysically relevant range of partition coefficient K and bulk composition x.

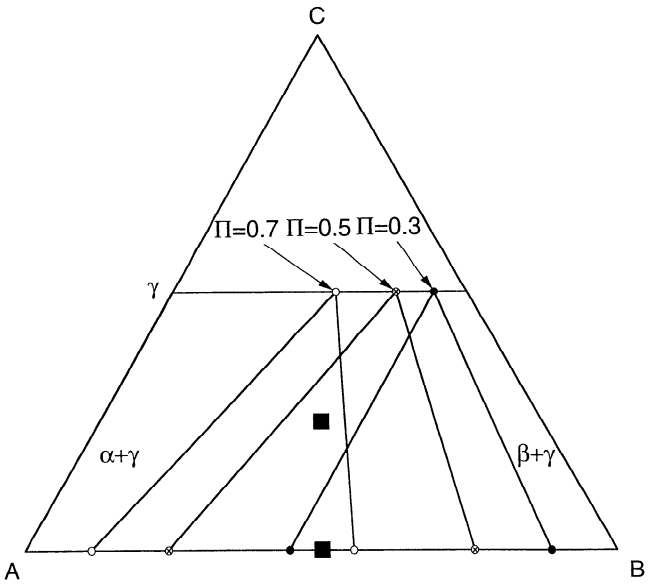

Figure 7. Schematic explanation of the effect of nontransforming phases. An isothermal ternary phase diagram is shown with components, A, B, C. Three isobaric sections of the three-phase α, β, γ coexistence region are shown. A bulk composition lying on the AB binary (bottom solid square), lies within all three three-phase coexistence regions. A bulk composition containing C (upper solid square) lies only within the two coexistence regions corresponding to the higher and middle pressures. The pressure interval over which three-phase coexistence exists in the three-component bulk composition is reduced relative to the binary case. The coexistence regions are calculated by assuming $K_{\alpha\beta}=K_{\alpha\gamma}=0.1$ at normalized pressures $\Pi=0.3$ (solid circles) $\Pi=0.5$ (circled crosses), and $\Pi=0.7$ (open circles). The parameters chosen are relevant to the transformation of olivine to wadsleyite in the presence of pyroxene in relatively cold subduction environments. In this case, the components and phases are identified as follows: A, Mg_2SiO_4; B, Fe_2SiO_4; C, SiO_2; α, olivine; β, wadsleyite; γ, pyroxene.

transforms to wadsleyite in the presence of $(Mg,Fe)SiO_3$ clinopyroxene. For unit partitioning between high-pressure and nontransforming phases, a reasonable approximation to the olivine-wadsleyite transition in the mantle,

$$f_\beta(\Pi) = \frac{f_{\beta 1}(\Pi)}{F_T} - \frac{1-F_T}{F_T} \qquad K_1 = K \qquad (18)$$

where $f_T f_{\beta 1}(\Pi)$ is the mole fraction of the high-pressure phase $\beta 1$, f_T is the mole fraction undergoing transformation, and $f_{\beta 1}(\Pi) = (x - x_{\alpha 1})/(x_{\beta 1} - x_{\alpha 1})$ is given by the equation for the bare binary case (12).

Figures 8 and 9 show that the nontransforming phase can have a substantial effect on the width of the phase loop and on the structure of the phase transition. For $x < 0.5$ and $K_1 \leq 1$, the nontransforming phase narrows the width of the coexistence region by delaying its onset to higher pressures. For parameters approximating the olivine-wadsleyite transition in relatively cold, subduction environments ($K = K_1$=0.1, x=0.1) the width of the transition region is reduced by more than a factor of 5 relative to the binary case, while the pressure at which the transformation begins is increased by $\Pi = 0.2$ or 20% of ΔP. The width of the transition region approaches zero as K_1 approaches zero; only if $K_1 > 1$ is the transition broadened by the nontransforming phase.

More Than Two Transforming Phases

In this section we examine pseudo-binary transitions involving more than two transforming phases, of which spinel to perovskite + magnesiowüstite is an example. This case was also explored by *Jeanloz and Thompson* [1983].

The equations for the form of the phase loop and the yield of the high-pressure assemblage are derived in Appendix B. We consider the case of equilibrium coexistence among n low-pressure and m high-pressure phases; all phases are assumed to be ideal binary solid solutions with mixing on one type of atomic site. The yield of the high-pressure assemblage

$$f_\beta(\Pi) = \frac{x(1-K) - C_A^{-1} K_g^{\Pi-1} K + K}{1 - C_A K_g^{1-\Pi} - C_A^{-1} K_g^{\Pi-1} K + K} \qquad (19)$$

In the multiphase case, K_g (B10) plays the role that the partition coefficient did in the binary case: it is independent of composition for ideal solutions and is independent of pressure to lowest order in δv. K_g is

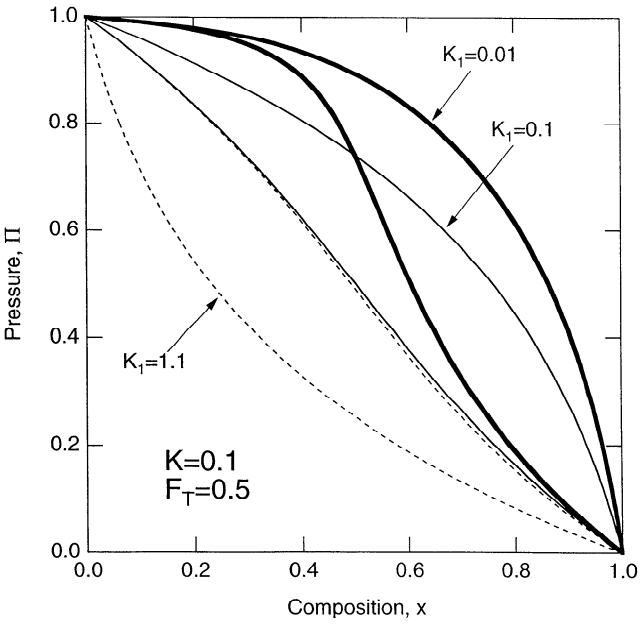

Figure 8. Pseudobinary coexistence of low- and high-pressure assemblages in a system with a single nontransforming phase. The proportion of solid solution species (A or B atoms) in the transforming fraction is F_T=0.5, the partition coefficient between transforming phases is K=0.1 (all curves), while that between phase $\alpha 1$ and the nontransforming phase γ is K_1=0.01 (bold), K_1=0.1 (thin), K_1=1.1 (dashed).

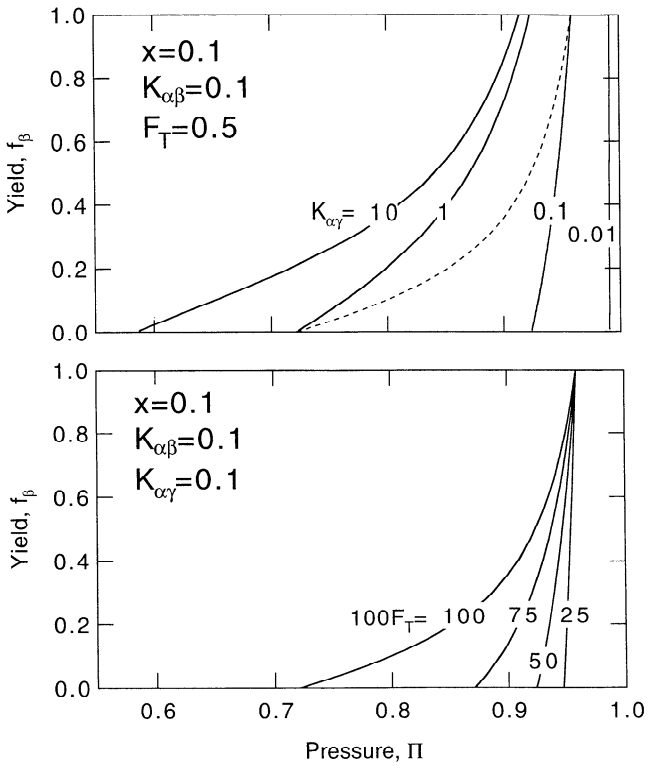

Figure 9. Effect of a single nontransforming phase on the yield of the high-pressure assemblage (f_β). (top) The effect of varying the partition coefficient between $\alpha 1$ and the nontransforming phase γ, K_1, is shown for a bulk composition x=0.1 and partitioning between transforming phases K=0.1, and F_T=0.5. The dashed line, shown for comparison, is the bare binary case (12) with $K = 0.1$ and $x = 0.1$. (bottom) The effect of varying F_T shown for fixed values of $x = 0.1$, $K = 0.1$, and $K_1 = 1.0$.

related to the partition coefficient K by the correction factors C_A and C_B which account for the difference between arithmetic and geometric mean compositions of reactant and product assemblages (B6). Equation (19) properly reduces to the result for a two-phase system (12) for $n = m = 1$, in which case $C_A = 1$, and $K_g = K$.

Unlike the binary case, the multiphase case must be solved numerically. Despite the more complex functional form, the pressure dependence of f_β is qualitatively similar to that of the binary case: it is still nonlinear and sigmoidal. Furthermore, as we show in the following example, many of the properties of the transition including its width and structure are similar to the binary case for a geophysically relevant range of parameters.

We consider a transition from one reactant phase (α) to two product phases ($\beta 1$,$\beta 2$), for which s_α=2, $s_{\beta 1} = s_{\beta 2} = 1$, $\nu_\alpha = \nu_{\beta 1} = \nu_{\beta 2} = 1$, and N=2. These parameters are appropriate to the spinel to perovskite + magnesiowüstite transition. Figure 10 shows that the three-phase case properly reduces to the binary case in the limit $K_{\beta 1 \beta 2}$=1. The form of the phase loop is relatively insensitive to partitioning within the high-pressure assemblage. For a bulk composition $x = 0.1$ and $K_{\beta 1 \beta 2}$=0.1, a probable lower bound on the partition coefficient between magnesiowüstite and perovskite [*Fei et al.*, 1991; *Katsura and Ito*, 1996], the width of the phase loop differs by only 20% from the binary case. The form of the phase loop and of $f_\beta(\Pi)$ are unchanged if $K_{\beta 1 \beta 2}$ is replaced by $K_{\beta 2 \beta 1} = 1/K_{\beta 1 \beta 2}$.

Multicomponent Phase Transitions

While a number of major mantle phases are essentially binary solid solutions, several important phase

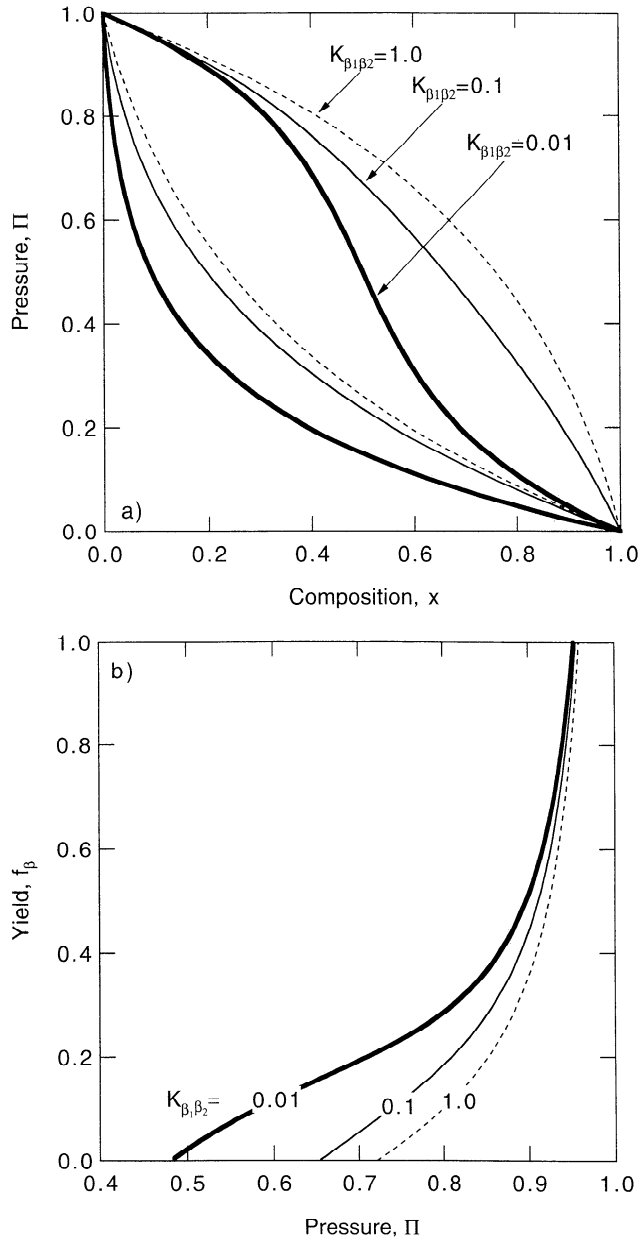

Figure 10. (a) Binary coexistence regions and (b) yield of the high-pressure phase for the three-phase pseudobinary transition discussed in the text. The geometric average partition coefficient K_g=0.1 (all curves) and that between the two high-pressure phases $K_{\beta 1 \beta 2}$=0.01 (bold), $K_{\beta 1 \beta 2}$=0.1 (thin), and $K_{\beta 1 \beta 2}$=1.0 (dashed). The bulk composition in Figure 10b is $x = 0.1$.

transitions involve more than two components. The pyroxene to garnet and the garnet to perovskite transitions, for instance, involve Ca- and Al-bearing species in addition to Mg- and Fe-bearing end-members. We consider the case of a transition between phases α and β each consisting of multicomponent substitutional solid solution on a single atomic site. An example of a phase transition which is described by this analysis is the pyroxene to garnet transition in the $M_3Al_2Si_3O_{12}$ system (M=Mg,Fe,Ca,...), where solid solution occurs only on the dodecahedral (octahedral) site in garnet (pyroxene). The pyroxene to garnet transition in the mantle is more complex as it involves solid solution on a second site: Al-Si-M solution takes place on the octahedral site in garnet and the tetrahedral site in pyroxene. Once the activities of all relevant components are properly defined, it is straightforward to generalize the analysis below to this more complex case, although we will not do so here. Instead, we will focus on the simple case of solution on one type of atomic site in order to illustrate the effects of multicomponent solution on the expected structure of phase transitions.

The equations for the form of the coexistence regions and the yield of the high-pressure assemblage are derived in Appendix C. We consider a transition from a low-pressure phase α to a high-pressure phase β. Each phase is assumed to be an N-component ideal solution, with solid solution on one type of atomic site. The yield of the high-pressure phase is given implicitly by

$$\sum_{i=1}^{N} \frac{x_i}{f_\beta(\Pi) + [1 - f_\beta(\Pi)]K^{\Pi - \Pi_i}} = 1 \qquad (20)$$

where x_i is the bulk composition vector, Π_i $(i = 1, N)$ are the end-member transition pressures, ordered such that $\Pi_1 > \Pi_2 > ... > \Pi_N$ and the partition coefficient $K = K_{1N}$. Equation (20) is easily solved numerically once the bulk composition (x_i) the end-member transition pressures, and the partition coefficient are specified. The width and structure of the transition differ from the binary case because of the additional components. However, the nonlinear, sigmoidal shape of the transition is preserved.

As an example, we consider the three-component case. We focus on strong partitioning ($K = 0.01$), because this is characteristic of the pyroxene to garnet and garnet to perovskite transitions. The structure of $f_\beta(\Pi)$ properly reduces to the binary case in the limit $x_A = x_C$, $x_B = 0$ (Figure 11a). Adding a third component to an equimolar mixture does not change the structure of the transition qualitatively: the transition is narrowed somewhat (by up to 20%) and is smoothed (made more linear) relative to the binary case (Figure 11a). Variations in Π_B also do not have a large effect on the structure of the transition: Figure 11b shows that varying Π_B from 0 to 1 changes the width of the transition by less than 15%. Figure 11c shows the effect of varying the ratio x_A/x_C while keeping x_B constant. The coexistence region shifts upward in pressure as the ratio increases, and the shape of the transition is affected, but the width changes little (less than 20%).

Phase Transitions in the Mantle

We have focused on ideal solutions in order to gain a general understanding of the expected structure of phase transitions without restricting ourselves to particular solution models. However, the solution properties of major mantle minerals are, for the most part, demonstrably nonideal, and we examine the effects of this behavior on the structure of mantle discontinuities in this section. Next, we examine the possible deviations from isothermal conditions under which phase transitions take place in the mantle and the effect of temperature gradients on discontinuity structure. Finally, because elastic waves are the primary probe of discontinuity structure, we consider in more detail the effective elastic properties of the multiphase composite which exists within the discontinuity region.

Nonideal Solutions

For nonideal solutions the activity coefficients (5) differ from unity. Defining

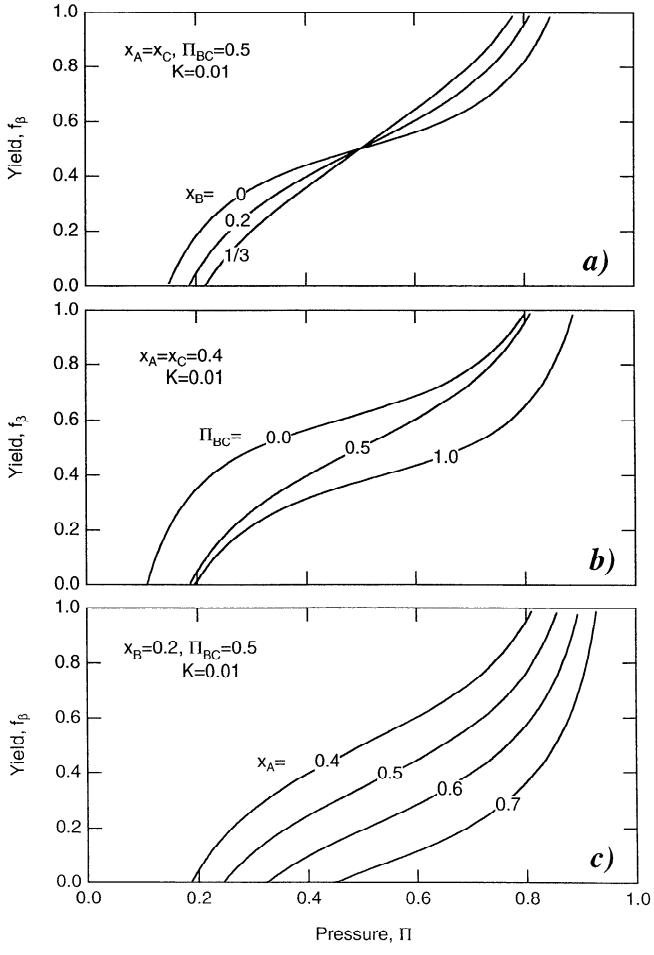

Figure 11. The effect of a third component on the yield of the high-pressure phase. (a) The effect of adding a third component B to an equimolar A-C binary mixture for fixed values of the A-C partition coefficient, K=0.01, and of the normalized B-C transition pressure, Π_{BC}=0.5. (b) The effect of varying Π_{BC} for fixed bulk composition and K. (c) The effect of varying the relative proportions of A and C for fixed x_B, Π_{BC}, K.

Table 2. Regular Solution Parameters w_A and w_B Defined by *Akaogi et al.* [1989] for Various Mantle Phases Consisting of Solid Solutions of Components A and B

Phase	A	B	w_A, J mol^{-1} K^{-1}	w_B, J mol^{-1} K^{-1}	Ref.
Olivine	Mg_2SiO_4	Fe_2SiO_4	6,320 (P)	8,320 (P)	1
			10,220	6,020	2
			6,100	6,100 (Sym.)	3
Wadsleyite	Mg_2SiO_4	Fe_2SiO_4	1,000	2,000	1
			3,900	3,900	2
			3,900	3,900 (Sym.)	3
Spinel	Mg_2SiO_4	Fe_2SiO_4	1,840 (T)	3,900	1
			3,900	3,900	2
			2,800	2,800 (Sym.)	3
			4,000	4,000 (Sym.)	4
Perovskite	$MgSiO_3$	$FeSiO_3$	4,200 (P,T)	4,140 (P,T)	1
			14,000	14,000 (Sym.)	4
Magnesiowüstite	MgO	FeO	16,100	15,900 (T)	1
			13,100	13,100 (Sym.)	3
			14,000	14,000 (Sym.)	4

Notations: (P) pressure-dependent parameter evaluated at the pressure of the closest major mantle discontinuity to the stability field, P=14 GPa for olivine, wadsleyite, and spinel, and P=24 GPa for perovskite and magnesiowüstite; (T) temperature-dependent parameter evaluated at T=1873 K; (Sym.) Symmetric regular solution model assumed (w_A=w_B). References: 1, *Fei et al.* [1991]; 2, *Akaogi et al.* [1989]; 3, *Stixrude and Bukowinski* [1993]; 4, *Wood* [1990].

$$\gamma_A = \frac{\gamma_A^\beta}{\gamma_A^\alpha}\ ,\ \gamma_B = \frac{\gamma_B^\beta}{\gamma_B^\alpha}\ ,\ \Gamma = \frac{\gamma_A}{\gamma_B} \tag{21}$$

we find that the product ΓK, rather than the partition coefficient itself, is independent of pressure to first order in $\delta v/v$ (compare (7)) The partition coefficient is now, in general, a function of pressure, temperature, and composition. The yield of the high-pressure phase is

$$f_\beta(\Pi) = \frac{x(1-K) - \gamma_B(\Gamma K)^\Pi + K}{1 - (\Gamma K)^{1-\Pi}/\gamma_A - \gamma_B(\Gamma K)^\Pi + K} \tag{22}$$

which must be determined numerically since the activity coefficients depend on composition. To illustrate the effects of nonideality, we examine the regular solution model, commonly used to approximate the nonideal solution properties of mantle phases [*Akaogi et al.*, 1989; *Wood*, 1990; *Fei et al.*, 1991]. In its symmetric form the model is defined by the activity coefficients

$$\gamma_i^j = \exp\left[\frac{w_j(1-x_i^j)^2}{RT}\right] \tag{23}$$

For most mantle minerals the solution parameters w_j are generally positive and range in magnitude from zero (ideal solution) to values comparable to RT at mantle temperatures (Table 2).

The primary effect of nonideality is to change the overall width of the coexistence region, rather than the form of pressure dependence of the yield. The effect of nonideality can be substantial for $w/RT > 1/4$ (Figure 12a). However, normalizing the pressure to the width of the coexistence region for the composition of interest ($P_\alpha(x) - P_\beta(x)$, see Figure 1) we find that even for

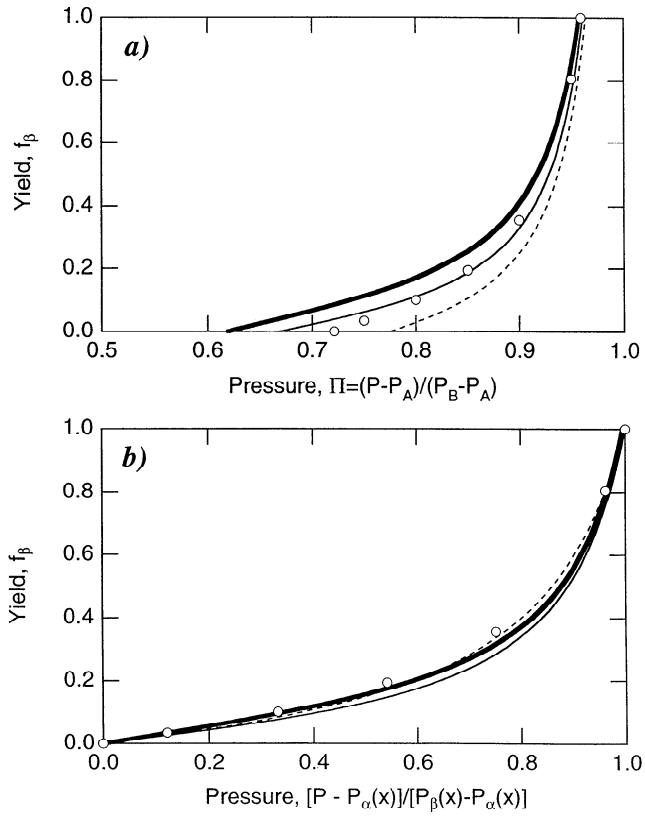

Figure 12. The effect of nonideality on the yield of the high-pressure phase is shown for a bulk composition, x = 0.1 and ΓK=0.1 for the ideal case (W_A=W_B=0, open circles), and nonideal cases: W_A=$RT/2$, W_B=0 (bold), W_A=0, W_B=$RT/2$ (dashed), W_A=W_B=$RT/2$ (thin). (a) The pressure is normalized by the pressure interval for which coexistence occurs ($P_A - P_B$). (b) The pressure is normalized by the interval of coexistence for the bulk composition of interest, x=0.1 ($P_\alpha(x) - P_\beta(x)$).

large values of w/RT the shape of the transition is not qualitatively affected.

The result that nonideality affects the width rather than the shape of a transition is important because the width is often known experimentally or can be estimated from other data. Typically, we will be interested in the pressure dependence of the yield of the transition for a known overall width. In this situation the ideal solution approximation suffices for most applications, even when the activities deviate by large amounts from ideal behavior. It is important to consider nonideality if the activity of a species is constrained independently, for instance, by calorimetric data. While such data are readily incorporated within the formalism outlined in this section, direct experimental constraints on activities, especially at high-pressure, are rare. Nonideality can have qualitatively important effects if it is large enough to cause a miscibility gap (as in plagioclase feldspars) or an azeotropic transition, of which the spinel to perovskite + magnesiowüstite transition may be an example (as implied by the calculated phase diagram of *Wood* [1990]).

Nonisothermal Conditions

Throughout most of the mantle, the geothermal gradient is expected to be approximately adiabatic and small (< 0.5 K km^{-1}). In the vicinity of mantle phase transitions the geothermal gradient can be greater. However, for most mantle phase transitions and probable geothermal gradients, our isothermal analysis is expected to be a good approximation to the widths of transition regions in the Earth.

To first order in their difference, geothermal W_{geo} and isothermal W_{iso} widths are related by

$$W_{\mathrm{geo}} = W_{\mathrm{iso}} \left[1 + \frac{1}{\rho g} \left(\frac{\partial P}{\partial T} \right)_{\mathrm{eq}} \left(\frac{\partial T}{\partial z} \right)_{\mathrm{geo}} \right] \qquad (24)$$

where $(\partial P/\partial T)_{\mathrm{eq}}$ is the Clapeyron slope of the phase transition, $(\partial T/\partial z)_{\mathrm{geo}}$ is the geothermal gradient, ρ is the density, and g is the acceleration due to gravity. For typical Clapeyron slopes and geothermal gradients tenfold greater than normal mantle, nonisothermal and isothermal widths can differ by 30%.

There are two reasons to expect greater than normal geothermal gradients in the vicinity of phase transitions. First is the *Verhoogen* [1965] effect, the refraction of the mantle adiabat due to the exchange of latent heat of transformation with the surroundings such that $(\partial T/\partial z)_{\mathrm{geo}}$ and $(\partial P/\partial T)_{\mathrm{eq}}$ have the same sign in the vicinity of the phase transition For values of the Clapeyron slope (3 MPa/K) and heat capacity (1000 J/kg K) appropriate for the olivine-wadsleyite transition, the adiabatic width is 5 km greater than the isothermal width [*Jeanloz and Thompson*, 1983]. This is likely an overestimate of the effect, however. In the case of relatively narrow transitions, the Verhoogen effect is expected to be nearly offset by thermal diffusion *Jeanloz and Thompson*, 1983]. For very broad transitions, such as pyroxene to garnet, thermal diffusion will be less important, but the broadening will be small compared with the width of the transition and, in terms of seismic reflectivity modeling, probably negligible compared with uncertainties in the shape of the transition.

Second, phase transitions may modify the geotherm through their effect on mantle flow. Endothermic phase transitions may inhibit vertical mass flux and cause superadiabatic temperature gradients to develop. According to (24) this effect will tend to reduce the width of the transition relative to the isothermal case. Superadiabatic temperature gradients may extend over several hundred kilometers in depth and may be overlain by a region of subadiabatic, or subisothermal, temperature gradients. If the 660 km discontinuity occurs in the superadiabatic region and the 410 km discontinuity in the subadiabatic region, both transitions will tend to be sharpened. However, fluid dynamical calculations [*Tackley et al.*, 1993] indicate that deviations from adiabaticity in the region of the phase change do not have a large effect on transition widths. Computed superadiabatic gradients are approximately 5 times normal which would change the width of a typical transition by approximately 15% relative to the isothermal case.

Composite Elastic Properties

The aggregate seismic velocity at any depth within the coexistence region will be, in general, a nonlinear function of f_β [*Watt et al.*, 1976]. However, phase transitions in the mantle generally involve coexisting phases which have similar seismic velocities. In this case, the yield of the high-pressure phase is an excellent approximation to the velocity structure of the discontinuity. If we assume that the difference in seismic wave velocities, $\delta v = v_\beta - v_\alpha$, is small (e.g., that $\delta v/v_\beta << 1$), we find that

$$\frac{v_{VRH} - v_\alpha}{v_\beta - v_\alpha} = f_\beta - \frac{1}{2} f_\beta (1 - f_\beta) \frac{\delta v}{v_\beta} \qquad (25)$$

where v_{VRH} is the Voigt-Reuss-Hill average of the extremal bounds on the aggregate velocity, v_α and v_β are the isotropically averaged seismic wave velocities of low- and high-pressure phases, respectively, and f_β is given by (12). To lowest order in the velocity difference, the normalized velocity structure of a phase transition is identical to (12). The first-order correction (second term on right-hand side) is everywhere less than $\delta v/8v_\beta$. For typical mantle discontinuities this correction term amounts to less than 1%. Given current uncertainties in the widths and partition coefficients of the relevant phase transitions, accounting for this correction term is probably not justified and will be ignored in the applications below (*Helffrich and Bina* [1994] also make this approximation). These conclusions may not hold if substantial anisotropy exists in the transition region, for instance, as a result of lattice-preferred orientation (texturing) produced by mantle flow. By analogy with large anisotropy observed in the surface dynamical boundary layer, significant anisotropy may develop in the neighborhood of 660 km if the corresponding phase transformation presents a substantial barrier to flow.

Applications and Discussion

We apply our results on the shape of mantle discontinuities to an analysis of the sharpness and possible reflectivity properties of the olivine to wadsleyite transition and to the garnet to perovskite transition. The former is expected to be the cause of the 410 km seismic discontinuity, while the latter may be the origin of seismic reflectivity near 710 km depth.

Olivine to Wadsleyite Transition

To determine the structure of the phase transition from (12), we need to estimate the partition coefficient K and pressure interval ΔP of binary coexistence, the mole fraction f_T of transforming phases, and the partition coefficient K_1 between transforming and nontransforming phases. We represent experimental measurements of K and W *Katsura and Ito* [1989] in terms of the present analysis as follows:

$$K = K_0 \exp\left[-\frac{A}{R}\left(T^{-1} - T_0^{-1}\right)\right] \tag{26}$$

$$W = \Delta P\left\{1 - \frac{\ln\left[K + x(1-x)(1-K)^2\right]}{\ln[K]}\right\} \tag{27}$$

where K_0 is the value of the partition coefficient at T_0. For $x = 0.1$, T_0=1873, the parameters K_0=0.55, ΔP=10.2 GPa or 256 km, and A/R=3297 K reproduce the experimental results of *Katsura and Ito* [1989] and their empirical expression for the temperature dependence of the width over a wide range of temperatures (Figure 13). We recognize that our representation of the temperature dependence of W is oversimplified. In particular, ΔP will be temperature-dependent as well, an effect which is essentially absorbed in our assumed temperature dependence of K. In any case, our primary concern here is the interpolation of experimental measurements: the currently available data do not warrant a more complex form. Nevertheless, it is important to recognize that the analysis in the preceding sections permits completely general expressions for the T dependence of W and K which may be introduced when more data are available.

To estimate f_T, we approximate the upper mantle as a two phase system in which the nonolivine (residuum) fraction is represented by a single phase of pyroxene stoichiometry. The bulk composition is approximated by the MgO-FeO-SiO_2 fraction. A more detailed treatment of the residuum, including explicit consideration of Al_2O_3 and CaO components, or explicit consideration of multiple phases (clinopyroxene, orthopyroxene, garnet) will affect the structure of the olivine to wads-

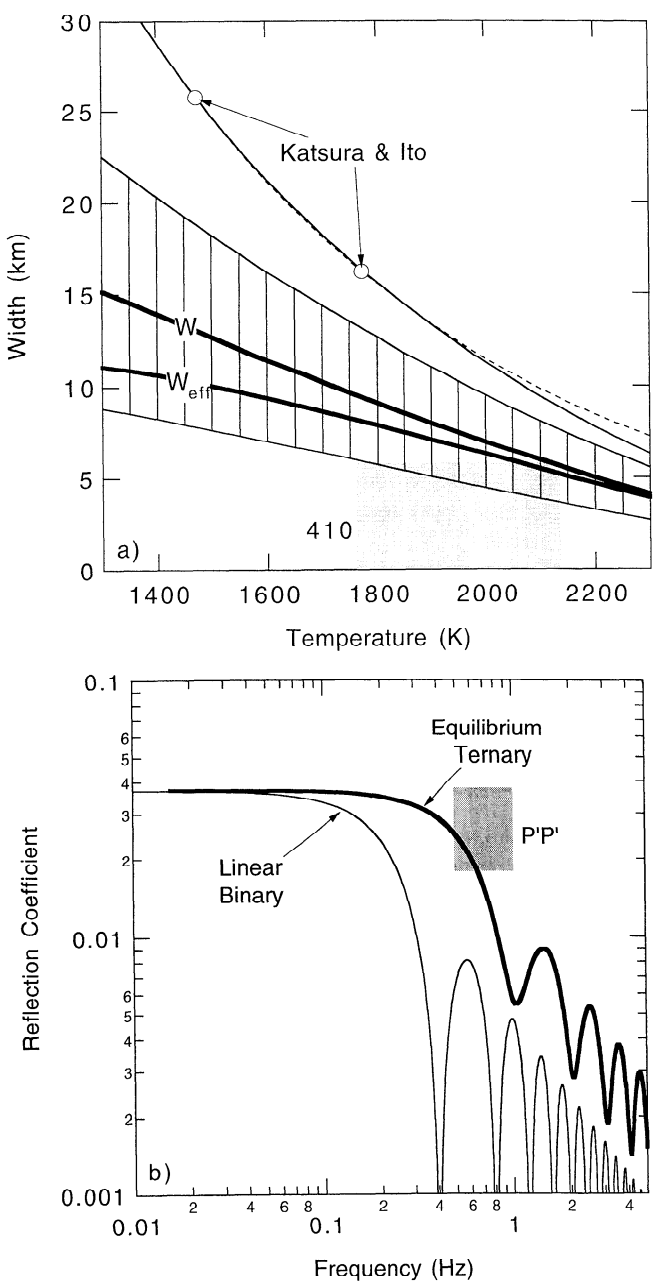

Figure 13. (a) The width of the olivine to wadsleyite transition in the mantle and (b) its reflection coefficient for near-normal incidence underside P wave reflections. In Figure 13a the predicted total width of the olivine to wadsleyite transition in the presence of a nontransforming phase (W) and its effective width (W_{eff}) are compared with geophysical constraints (shaded box) on the maximum width of the discontinuity (see text) and the temperature at 410 km depth [*Brown and Shankland*, 1981; *Jeanloz and Knittle*, 1989; *Morishima et al.*, 1994]. Hatching represents uncertainties in W: the lower bound corresponds to $K_1 = K/2$, and the upper bound corresponds to $K_1 = 2K$. The effective width is calculated with $K = K_1$. The top curves represent the width of the binary olivine to wadsleyite transition according to (12) (thin solid line) and the measurements and empirical expression of *Katsura and Ito* [1989] (circles, thin dashed line). In Figure 13b the P wave reflectivity of the olivine to wadsleyite transition is compared with high-frequency observations of underside $P'P'$ reflections (*Benz and Vidale* [1993]; shaded box). For comparison, the reflectivity of a linear approximation to the bare binary case is also shown (light line).

leyite transition little. For pyrolite, the mole fraction of olivine is $f_T \approx 0.6$. With the stoichiometric coefficients, s_T=2, and s_1=1, we have F_T=0.7 from (A3). We focus on a pyrolite bulk composition here because it yields a conservative estimate of the width of the transition. A piclogitic composition ($F_T \approx 0.5$) will yield narrower widths than those estimated below.

We estimate the partition coefficient between olivine and nonolivine fractions from the data of *Akaogi and Akimoto* [1979]. They find approximate equipartitioning of Fe between wadsleyite and residuum, indicating that the corresponding partition coefficient $K_{\beta-\mathrm{res}} \approx 1.0$. We then have for the partition coefficient between olivine and residuum, $K_{\alpha-\mathrm{res}} = K_1 \approx K$. Because the temperature dependence of K_1 is not known, nor its dependence on the Ca or Al content of the residuum, we explore a range of values of this parameter: $K/2 < K_1 < 2K$. The effects of other possible sources of uncertainty, including experimentally measured temperatures, which may be underestimated by 100 K [*Morishima et al.*, 1994], are likely to be smaller than those associated with K_1. The total width of the three phase coexistence region and its effective width is calculated using (15)-(17).

The results show that the total width of the olivine + wadsleyite + residuum coexistence region is half that of the binary transition (Figure 13a). This means that the width of an experimentally determined binary phase loop substantially overestimates the width of the transition in the mantle. The effective width W_{eff} is narrower still, amounting to 40% of the width of the binary phase loop. For typical transition zone temperatures the effective width of the transitions lies between 4 and 8 km. This is consistent with the maximum width of an equivalent linear discontinuity (4-6 km) found in studies of reflections from the 410 km discontinuity [*Whitcomb and Anderson*, 1970; *Leven*, 1985; *Benz and Vidale*, 1993].

To investigate the reflective properties of the olivine to wadsleyite transition in more detail, we have computed its frequency dependent underside P wave reflection coefficient (Figure 13b). The reflection coefficient is calculated from (17) with $x = 0.1$, $F_T = 0.7$, $\Delta P = 256$ km, and $K = 2K_1 = 0.62$, appropriate to transition zone temperatures. The zero frequency P wave impedance contrast (3.7%) is taken to be that of the 410 km discontinuity in the preliminary reference earth model (PREM) [*Dziewonski and Anderson*, 1981]. We find that the reflection coefficient for 1 Hz P waves is approximately 0.6% and for 0.5 Hz P waves is 2.5%, in the range of that observed [*Benz and Vidale*, 1993]. While recognizing that uncertainties remain (especially in K_1), our analysis shows that the properties of the equilibrium olivine to wadsleyite transition are at least marginally consistent with the highest-frequency observations of seismic reflections from 410 km discontinuity.

The predicted temperature dependence of the effective width of the transition provides a possible explanation for the intermittent visibility of the 410 km discontinuity in studies of reflected phases. Figure 13a predicts that the 410 km discontinuity should reflect more short-period energy in relatively high temperature mantle and that it may be invisible to short-period waves in cold mantle. This explanation for intermittent visibility was also advanced by *Helffrich and Bina* [1994].

Our explanation of the sharpness of the 410 km discontinuity in terms of equilibrium thermodynamics has the advantage that it does not postulate untested or poorly constrained physical properties or processes. The effects of nonequilibrium thermodynamics may also contribute to the sharpness of the 410 km discontinuity [*Solomatov and Stevenson*, 1994], although our analysis indicates that any sharpening in addition to that predicted in equilibrium need not be large to explain the seismological data. Nonequilibrium models of the shape of the discontinuity depend critically on the effective surface tension, a quantity which is currently unknown in the Mg-silicate olivine system, but which could be measured, providing important constraints on the importance of nonequilibrium effects.

A univariant transition in the MgO-FeO-SiO_2 system [*Jeanloz and Thompson*, 1983] is unlikely to occur in most of the mantle for generally accepted models of upper mantle composition. For the olivine + spinel to wadsleyite + spinel univariant transition to explain the 410 km discontinuity, the Fe content of the mantle must exceed Fe/(Mg+Fe)> 0.16 in normal temperature mantle (1900 K) and 0.12 in relatively cold (1500 K) mantle [*Katsura and Ito*, 1989]. The iron content required for normal mantle is substantially larger than that generally accepted on the basis of constraints provided by the analysis of xenoliths, genesis of basalt, and the comparison of observed seismic velocities in the mantle and estimates of elastic wave velocities of candidate upper mantle compositions.

Garnet to Perovskite Transition

We treat this transition approximately in the binary enstatite-pyrope system, for which there are the most experimental constraints. We neglect the effects of FeO, which may be important [*O'Neill and Jeanloz*, 1994] but which are less well constrained. We represent the experimental results in the iron-free system [*Irifune and Ringwood*, 1987; *Irifune et al.*, 1996] by assuming that garnet and perovskite are binary solid solutions consisting of enstatite and pyrope composition end-members which mix ideally on a single atomic site. Our solution model neglects probable multiatom mixing on the octahedral site in garnet (Mg,Si,Al) and does not explicitly distinguish between potential mixing sites in perovskite (octahedral, dodecahedral). Nevertheless, our simplified model reproduces the available data on the transition and is expected to capture its basic features.

The experimentally determined pyrope contents of coexisting garnet and perovskite [*Irifune and Ringwood*, 1987; *Irifune et al.*, 1996] imply a partition coefficient $K \approx 0.03$ at 1773 K. As there are no data on the temperature dependence of K, we assume that

$$K = \exp\left[-\frac{A}{RT}\right] \tag{28}$$

with A/R=6200 K, which reproduces the experimental result. From Irifune and Ringwood's estimate of the garnet to perovskite transition pressure in the pyrope end-member and from measurements of the transition in the enstatite end-member [*Gasparik*, 1990], we estimate ΔP=8.5 GPa or 190 km. For the bulk composition appropriate for a pyrolite mantle (x_{en} = 0.8), these parameters yield a total transition width, W=4.4 GPa, or 100 km. A linear transition of this width is unlikely to reflect significant seismic energy. However, the effective width of the transition is much less.

From the curves in Figure 6, we find that the effective width is 30% of W, so that $W_{\text{eff}} \approx 30$ km (Figure 14). The effective width increases slightly as the partition coefficient approaches unity with increasing temperature. This means that the garnet to perovskite transition is expected to reflect significant amounts of seismic energy with wavelengths as small as $\approx$ 100 km, over the entire temperature range typical of the uppermost lower mantle.

We propose that the garnet to perovskite transition is responsible for seismological observations of reflections from 710 km depth [*Revenaugh and Jordan*, 1991]. The transition is known to occur in the appropriate depth range for plausible mantle compositions [*Irifune*, 1994]. To investigate the reflectivity of this transition in more detail, we have calculated its frequency-dependent SH reflection coefficient. The reflection coefficient is calculated from (12) with x = 0.8, ΔP=190 km, and K = 0.045, appropriate to uppermost lower mantle temperatures. The zero-frequency impedance contrast (6.2%) is taken from ambient pressure data on enstatite end-members [*Ita and Stixrude*, 1992; *Yeganeh-Haeri*, 1994; *Bass and Kanzaki*, 1990; *Yeganeh-Haeri et al.*, 1990] and reduced by the assumed fraction of enstatite+pyrope components in the mantle (30%). With these parameters the width and average velocity gradient of the garnet to perovskite transition are almost identical to the region of anomalously high velocity gradients in the PREM model between 670 and 771 km depth. The calculated reflection coefficient is in excellent agreement with those observed in studies of ScS reverberations in the frequency range 10-40 mHz [*Revenaugh and Jordan*, 1991]. For comparison, the reflection coefficient of the equilibrium transition is at least 4 times that of a linear transition of the same width.

Conclusions

We have shown that phase transitions in the mantle are much sharper than one would expect based on the width of binary coexistence regions. The nonlinear dependence of the yield of the high-pressure phase and the effects of nontransforming phases in the multicomponent mantle each act to narrow the region over which most of the transition occurs. The expected nonlinear structure of equilibrium phase transitions makes it possible for even broad transitions to reflect short-period energy. For example, the garnet to perovskite transition, though 100 km in width, is capable of reflecting

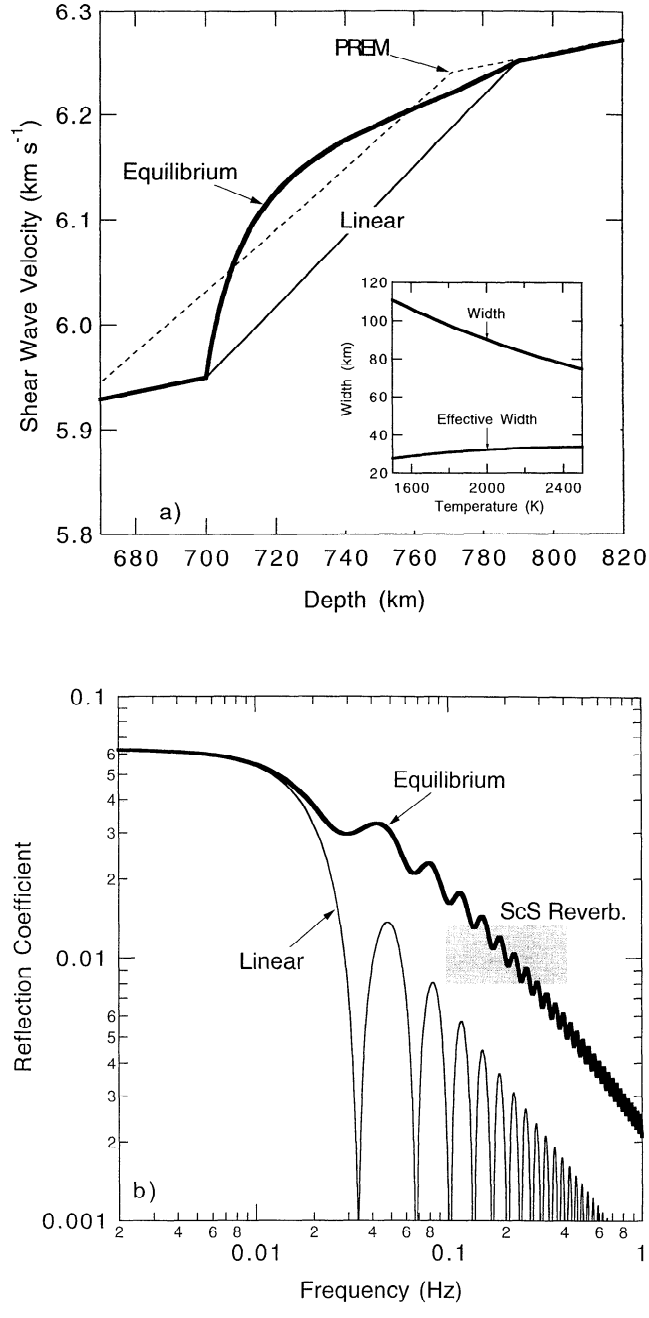

Figure 14. The (a) structure and (b) reflectivity of the garnet to perovskite transition. In Figure 14a the inset compares the total width W to the effective width W_{eff} of the garnet to perovskite transition as a function of temperature. The predicted S wave velocity structure of the transition is shown (bold line) for the 150 km below the 670 km seismic discontinuity in the PREM model (dashed line). The depth of the phase transition has been chosen such that $f_\beta = 2/3$ at 710 km, which is consistent with phase equilibrium data. The equilibrium structure of the transition is compared with a second-order (linear) discontinuity of the same width. In Figure 14b, predicted SH reflection coefficient (bold line) of the garnet to perovskite transition is compared with the observations of *Revenaugh and Jordan* [1991] (shaded box). The results are compared with the reflectivity of a linear transition of the same width as the phase transition (light line).

40 mHz S wave energy. Nontransforming phases act as buffers that can substantially reduce the total width over which a transition occurs: the width of the olivine to wadsleyite transitions is likely reduced by a factor of 2 by the presence of garnet and pyroxene in the mantle.

These results suggest a resolution of the apparent discrepancy between the widths of phase transitions and the reflectivity of seismic discontinuities. We propose that when multicomponent effects are taken into account, the equilibrium olivine to wadsleyite transition may be sufficiently sharp to explain seismic reflectivity observations and that special processes, or properties, such as large kinetic effects, are not required.

Our analysis leads to an explanation of a seismic discontinuity previously unaccounted for by a mantle phase transition. We suggest that the 710 km discontinuity is caused by the garnet to perovskite transition. Though its total width is large, its effective width is a factor of 3 less and is capable of reflecting S wave energy in the observed frequency range.

We have derived simple analytical expressions which depend essentially on a single parameter in the binary case, the partition coefficient K. Two parameters (two partition coefficients) are involved when the presence of a nontransforming phase is important. Future modeling of reflections and conversions expected from phase transitions should account for the expectations of equilibrium thermodynamics as embodied in these expressions.

Appendix A: Effect of Nontransforming Phases

We assume a transition from a low-pressure phase $\alpha 1$ to a high-pressure phase $\beta 1$ both of composition $(\mathrm{A,B})_{s_T}\mathrm{R}_z$. The transition takes place in the presence of nontransforming phases $\gamma 1$, $\gamma 2$, ...,γn, of composition $(\mathrm{A,B})_{s_j}\mathrm{C}_{cj}\mathrm{D}_{dj}$..., j=1,$n$. All phases are binary substitutional solid solutions with end-member components A and B. The mole fraction undergoing transformation is f_T, and the mole fractions of the nontransforming phases are f_1, f_2,...,f_n. The bulk compositions of the low- and high-pressure assemblages are then

$$x_\alpha = F_T x_{\alpha 1} + \sum_{i=1}^{n} F_i x_{\gamma i} \tag{A1}$$

$$x_\beta = F_T x_{\beta 1} + \sum_{i=1}^{n} F_i x_{\gamma i} \tag{A2}$$

where

$$F_T = \frac{f_T s_T}{f_T s_T + \sum_{j=1}^{n} f_j s_j}, \quad F_i = \frac{f_i s_i}{f_T s_T + \sum_{j=1}^{n} f_j s_j} \tag{A3}$$

are the relative proportions of A or B atoms in transforming and nontransforming phases, respectively.

Partitioning between phases is specified by $K_{\alpha_1\beta 1}$ and $K_{\alpha 1\gamma i}$ ($i = 1, ..., n$). For notational convenience, we will drop the unnecessary subscripts and write $K = K_{\alpha_1\beta 1}$ and $K_i = K_{\alpha 1\gamma i}$. From the definition of the partition coefficient and (A1) we have

$$x_{\gamma i} = \left[K_i \frac{1-x_{\alpha 1}}{x_{\alpha 1}} + 1\right]^{-1} = \frac{K^{\Pi} - K}{K_i(1 - K^{\Pi}) + K^{\Pi} - K} \tag{A4}$$

Substituting this expression into (A1) and (A2), we solve for the mole fraction of the high-pressure assemblage

$$f_\beta(\Pi) = \frac{x(1-K) - (K^{\Pi} - K)(1 - S_\gamma)}{F_T(1 - K^{1-\Pi} - K^{\Pi} + K)} \tag{A5}$$

where

$$S_\gamma = 1 - F_T - \sum_{i=1}^{n} F_i \frac{(1-K)}{K_i(1 - K^{\Pi}) + K^{\Pi} - K} \tag{A6}$$

which vanishes in the absence of nontransforming phases ($F_T = 1$).

Appendix B: More Than Two Transforming Phases

We assume that n reactant (low-pressure) phases, $\alpha 1$, $\alpha 2$, ..., αn, coexist in equilibrium with m product (high-pressure) phases, $\beta 1$, $\beta 2$, ..., βm. All phases are binary substitutional solid solutions with mixing on one type of atomic site. The generalized compositional formula of phase j can be written $(\mathrm{A}_{1-x_j},\mathrm{B}_{x_j})_{s_j}\mathrm{C}_{c_j}\mathrm{D}_{d_j}$..., j=$\alpha 1$, ..., αn, $\beta 1$, ..., βm. Mixing occurs on the atomic site occupied by the A and B atoms, and no mixing occurs on the sites occupied by C, D... The number of components (A, B, C,...) is dictated by the phase rule and the number of phases in coexistence. Each phase j has two components, A_j (formula $\mathrm{A}_{s_j}\mathrm{C}_{c_j}\mathrm{D}_{d_j}$...) and B_j ($\mathrm{B}_{s_j}\mathrm{C}_{c_j}\mathrm{D}_{d_j}$...). Unlike in the two-phase binary system, the components may have different compositions in different phases. Indeed, the phase rule demands this if more than two phases are in coexistence.

Equilibrium requires that the sum of the chemical potentials of component A and of component B be equal in the low-pressure and high-pressure assemblages:

$$\nu_{\alpha 1}\mu_B^{\alpha 1} + \nu_{\alpha 2}\mu_B^{\alpha 2} + ... + \nu_{\alpha n}\mu_B^{\alpha n} = \nu_{\beta 1}\mu_B^{\beta 1} + \nu_{\beta 2}\mu_B^{\beta 2} + ... + \nu_{\beta m}\mu_B^{\beta m} \tag{B1}$$

$$\nu_{\alpha 1}\mu_A^{\alpha 1} + \nu_{\alpha 2}\mu_A^{\alpha 2} + ... + \nu_{\alpha n}\mu_A^{\alpha n} = \nu_{\beta 1}\mu_A^{\beta 1} + \nu_{\beta 2}\mu_A^{\beta 2} + ... + \nu_{\beta m}\mu_A^{\beta m} \tag{B2}$$

where the ν_i are the coefficients that ensure mass balance. They are given by the relation

$$N = \sum_{j=1}^{n} \nu_{\alpha j} s_{\alpha j} = \sum_{j=1}^{m} \nu_{\beta j} s_{\beta j} \tag{B3}$$

where N is the total number of A or B atoms appearing

on each side of (B1) and (B2): the total number of A or B atoms must be equal for a consistent set of reactions.

The arithmetic mean compositions of the reactant assemblage

$$x_\alpha = 1/N \sum_{j=1}^{n} \nu_{\alpha j} s_{\alpha j} x_{\alpha j} \tag{B4}$$

where x_{α_j} is the mole fraction of component B in phase j. The geometric mean composition

$$\bar{x}_i^\alpha = \left[\prod_{j=1}^{p} (x_i^{\alpha_j})^{\nu_{\alpha_j} s_{\alpha_j}} \right]^{1/N} \tag{B5}$$

where i=A or B. The arithmetic and geometric mean compositions of the product assemblage are similarly defined. Correction factors

$$C_i = \frac{x_i^\beta}{x_i^\alpha} \frac{\bar{x}_i^\alpha}{\bar{x}_i^\beta} \tag{B6}$$

where i=A or B, account for the difference between arithmetic and geometric mean compositions (compare similar factors defined by *Jeanloz and Thompson* [1983]).

Recalling the definition of the chemical potential, substituting this into (B1) and (B2) and rearranging, we have

$$\frac{\bar{x}_B^\alpha}{\bar{x}_B^\beta} = \exp\left[\frac{-(P - P_B)v}{RT}\right] = K_g^\Pi \tag{B7}$$

$$\frac{\bar{x}_A^\alpha}{\bar{x}_A^\beta} = \exp\left[\frac{-(P - P_A)v}{RT}\right] = K_g^{(\Pi-1)} \tag{B8}$$

As in the binary analysis, P_A and P_B are the pressures of the phase transition in the end-member components. We have assumed that solution is ideal, that the phases can be approximated as incompressible over the region of coexistence, and that

$$\Delta V_i = \sum_{j=1}^{n} \nu_{\alpha j} V_i^{\alpha j} - \sum_{j=1}^{m} \nu_{\beta j} V_i^{\beta j} = Nv \tag{B9}$$

where i=A or B, and v is the volume of transition per A or B atom. The quantity

$$K_g = \frac{\bar{x}_B^\alpha \bar{x}_A^\beta}{\bar{x}_B^\beta \bar{x}_A^\alpha} = K \frac{C_B}{C_A} \tag{B10}$$

is independent of bulk composition in the ideal solution limit and is independent of pressure to lowest order in the difference $\Delta V_A - \Delta V_B$. K_g can also be written as a weighted geometric average of the interphase partition coefficients $K_{\alpha_i \beta_j}$ with weights given by the corresponding ν_i and s_i.

It is useful to rewrite these results in a way which makes the connection to the binary case more transparent. Combining (B7), (B8), and (B10),

$$x_\beta = \frac{1 - C_A K_g^{1-\Pi}}{1 - K} \tag{B11}$$

$$x_\alpha = \frac{C_A^{-1} K_g^{\Pi-1} K - K}{1 - K} \tag{B12}$$

and for the yield of the high-pressure assemblage,

$$f_\beta(\Pi) = \frac{x(1 - K) - C_A^{-1} K_g^{\Pi-1} K + K}{1 - C_A K_g^{1-\Pi} - C_A^{-1} K_g^{\Pi-1} K + K} \tag{B13}$$

Because K (and C_A and C_B) depend on x and P, it is actually more convenient to solve the multiphase case numerically, using (B7) and (B8). This is readily done once the values of the nm interphase partition coefficients $K_{\alpha i \beta j}$ are given.

Appendix C: Transitions Involving More Than Two Components

The generalized compositional formula of each phase, consisting of N components, 1, 2,..., N, is $(A_{x_1} B_{x_2} C_{x_3} ...)_s R_z$, such that the x_i sum to unity. The bulk composition is described by the mole fraction of each component, x_i, and the components are labeled such that the end-member transition pressures are ordered $P_1 > P_2 > ... > P_N$. Assuming, as before, ideal solutions and incompressibility over the pressure range of the phase transition, the N equations of equilibrium are

$$\mu_i^\alpha - \mu_i^\beta = (P - P_i)\Delta V_i + sRT \ln \frac{x_i^\alpha}{x_i^\beta} = 0 \tag{C1}$$

where i=1,2,...N. If we assume, as before, that all the ΔV_i are similar ($\Delta V_i/s = v$), then

$$K_{N1} = \exp\left[-\frac{(P_1 - P_N)v}{RT}\right] \tag{C2}$$

Defining the normalized pressure, $\Pi = (P - P_N)/(P_1 - P_N)$, and the normalized end-member transition pressures, $\Pi_i = (P_i - P_N)/(P_1 - P_N)$, and dropping the subscript on K_{N1}, the equations of equilibrium become

$$x_i^\alpha = x_i^\beta K^{\Pi - \Pi_i} \tag{C3}$$

or in terms of the bulk composition,

$$x_i^\beta = x_i \left[f_\beta + (1 - f_\beta) K^{\Pi - \Pi_i}\right]^{-1} \tag{C4}$$

where the yield of the high-pressure phase f_β is given by

$$\sum_{i=1}^{N} \frac{x_i}{f_\beta(\Pi) + [1 - f_\beta(\Pi)] K^{\Pi - \Pi_i}} = 1 \tag{C5}$$

The set of $N + 1$ equations (C4) and (C5) are readily solved numerically for the $N+1$ unknowns (x_i^β and f_β).

Acknowledgments. This work supported by the National Science Foundation under grants EAR-9305060 and EAR-9628199. I thank M. S. T. Bukowinski, R. Jeanloz, G. Helffrich, and an anonymous reviewer for their comments which improved the manuscript.

References

Akaogi, M., and S. Akimoto, High -pressure phase equilibria in a garnet lherzolite, with special reference to Mg^{2+}-Fe^{2+} partitioning among constituent minerals, *Phys. Earth Planet. Inter., 19*, 31-51, 1979.

Akaogi, M., E. Ito, and A. Navrotsky, Olivine-modified spinel-spinel transitions in the system Mg_2SiO_4-Fe_2SiO_4: Calorimetric measurements, thermochemical calculation, and geophysical application, *J. Geophys. Res., 94*, 15671-15685, 1989.

Aki, K., and P. G. Richards, *Quantitative Seismology*, vol. I, W. H. Freeman, New York, 1980.

Bass, J. D., and M. Kanzaki, Elasticity of a majorite-pyrope solid solution, *Geophys. Res. Lett., 17*, 1989-1992, 1990.

Benz, H. M., and J. E. Vidale, Sharpness of upper mantle discontinuities determined from high-frequency reflections, *Nature, 365*, 147-150, 1993.

Bina, C. R., and M. Kumazawa, Thermodynamic coupling of phase and chemical boundaries, *Phys. Earth Planet. Inter., 76*, 329-341, 1993.

Brown, J. M., and T. J. Shankland, Thermodynamic properties in the Earth as determined from seismic profiles, *Geophys. J. R. Astron. Soc., 66*, 579-596, 1981.

Duffy, T. S., and D. L. Anderson, Seismic velocities in mantle minerals and the mineralogy of the upper mantle, *J. Geophys. Res., 94*, 1895-1912, 1989.

Dziewonski, A. M., and D. L. Anderson, Preliminary reference Earth model, *Phys. Earth Planet. Inter., 25*, 297-356, 1981.

Fei, Y. W., H. K. Mao, and B. O. Mysen, Experimental determination of element partitioning and calculation of phase relations in the MgO-FeO-SiO_2 system at high pressure and high temperature, *J. Geophys. Res., 96*, 2157-2170, 1991.

Gasparik, T., Phase relations in the transition zone, *J. Geophys. Res., 95*, 15751-15769, 1990.

Hashin, Z., and S. Shtrikman, A variational approach to the elastic behavior of multiphase materials, *J. Mech. Phys. Solids, 11*, 127-140, 1963.

Helffrich, G., and C. R. Bina, Frequency dependence of the visibility and depths of mantle seismic discontinuities, *Geophys. Res. Lett., 21*, 2613-2616, 1994.

Irifune, T., and A. E. Ringwood, Phase transformation in a harzburgite composition to 26 GPa: Implications for dynamical behavior of the subducting slab, *Earth Planet. Sci. Lett., 86*, 365-376, 1987.

Irifune, T., Absence of an aluminous phase in the upper part of the Earth's lower mantle, *Nature, 370*, 131-133, 1994.

Irifune, T., T. Koizumi, and J. I. Ando, An experimental study of the garnet-perovskite transformation in the system $MgSiO_3$-$Mg_3Al_2Si_3O_{12}$, *Phys. Earth Planet. Inter., 96*, 147-157, 1996.

Ita, J. J., and L. Stixrude, Petrology, elasticity, and composition of the mantle transition zone, *J. Geophys. Res., 97*, 6849-6866, 1992.

Ito, E., and E. Takahashi, Postspinel transformations in the system Mg_2SiO_4-Fe_2SiO_4 and some geophysical implications, *J. Geophys. Res., 94*, 10637-10646, 1989.

Jeanloz, R., and E. Knittle, Density and composition of the lower mantle, *Philos. Trans. R. Soc. London, Ser. A, 328*, 377-389, 1989.

Jeanloz, R., and A. B. Thompson, Phase transitions and mantle discontinuities, *Revs. Geophys., 21*, 51-74, 1983.

Katsura, T., and E. Ito, The system Mg_2SiO_4-Fe_2SiO_4 at high-pressures and temperatures: precise determination of stabilities of olivine, modified spinel, and spinel, *J. Geophys. Res., 94*, 15663-15670, 1989.

Katsura, T., and E. Ito, Determination of Fe-Mg partitioning between perovskite and magnesiowüstite, *Geophys. Res. Lett., 23*, 2005-2008, 1996.

Kawakatsu, H., and F. Niu, Seismic evidence for a 920-km discontinuity in the mantle, *Nature, 371*, 301-305, 1994.

Kerrick, D. M., and L. S. Darken, Statistical thermodynamic models for ideal oxide and silicate solid solutions with application to plagioclase, *Geochim. Cosmochim. Acta, 39*, 1431-1442, 1975.

Lees, A. C., M. S. T. Bukowinski, and R. Jeanloz, Reflection properties of phase transition and compositional change models of the 670-km discontinuity, *J. Geophys. Res., 88*, 8145-8159, 1983.

Leven, J. H., The application of synthetic seismograms to the interpretation of the upper mantle P-wave velocity structure in northern Australia, *Phys. Earth Planet. Inter., 38*, 9-27, 1985.

Meijering, J. L., and C. J. M. Rooymans, On the olivine-spinel transition in the Earth's mantle, *Proc. Ned. Akad. Wetens., 61*, 333-344, 1958.

Morishima, H., T. Kato, M. Suto, E. Ohtani, S. Urakawa, W. Utsumi, O. Shimomura, and T. Kikegawa, The phase boundary between a- and b-Mg_2SiO_4 determined by in situ x-ray observation, *Science, 265*, 1202-1203, 1994.

O'Neill, B., and R. Jeanloz, $MgSiO_3$-$FeSiO_3$-Al_2O_3 in the Earth's lower mantle: Perovskite and garnet at 1200 km depth, *J. Geophys. Res., 99*, 19901-19915, 1994.

Revenaugh, J., and T. H. Jordan, Mantle layering from *ScS* reverberations, 2, The transition zone, *J. Geophys. Res., 96*, 19763-19780, 1991.

Richards, P. G., Seismic waves reflected from velocity gradient anomalies within the Earth's upper mantle, *Z. Geophys., 38*, 517-527, 1972.

Richter, F. M., Finite amplitude convection through a phase boundary, *Geophys. J. R. Astron. Soc., 35*, 265-276, 1973.

Shearer, P. M., Constraints on upper mantle discontinuities from observations of long-period reflected and converted phases, *J. Geophys. Res., 96*, 18147-18182, 1991.

Skinner, B. J., and F. R. Boyd, Aluminous enstatites, *Carn. Inst. Wash. Yearbook, 63*, 163-165, 1964.

Solomatov, V. S., and D. J. Stevenson, Can sharp seismic discontinuities be caused by nonequilibrium phase transformations?, *Earth Planet. Sci. Lett., 125*, 267-279, 1994.

Stixrude, L., and M. S. T. Bukowinski, Thermodynamic analysis of the system MgO-FeO-SiO_2 at high-pressure and the structure of the lowermost mantle, in *Evolution of the Earth and Planets, Geophys. Mon. Ser.* vol. 74, edited by E. Takahashi, R. Jeanloz, and S. Rubie, pp. 131-141, AGU, Washington, D. C., 1993.

Tackley, P. J., D. J. Stevenson, G. A. Glatzmeier, and G. Schubert, Effects of an endothermic phase transition at 670 km depth in a spherical model of convection in the Earth's mantle, *Nature, 361*, 699-704, 1993.

Verhoogen, J., Phase changes and mantle convection, *Philos. Trans. R. Soc. London, Ser. A, 258*, 276-283, 1965.

Vidale, J. E., and H. M. Benz, Upper-mantle seismic discontinuities and thermal structure of subduction zones, *Nature, 356*, 678-683, 1992.

Watt, J. P., G. F. Davies, and R. J. O'Connell, The elastic properties of composite materials, *Revs. Geophys., 14*, 541-563, 1976.

Weidner, D. J., A mineral physics test of a pyrolite mantle, *Geophys. Res. Lett., 12*, 417-420, 1985.

Whitcomb, J. H., and D. L. Anderson, Reflection of P'P' seismic waves from discontinuities in the mantle, *J. Geophys. Res., 75*, 5713-5728, 1970.

Wicks, C. W., and M. A. Richards, A detailed map of the 660-kilometer discontinuity beneath the Izu-Bonin subduction zone, *Science, 261*, 1424-1427, 1993.

Wood, B. J., Postspinel transformations and the width of the 670-km discontinuity: A comment on "Postspinel transformations in the system Mg_2SiO_4-Fe_2SiO_4 and some geophysical implications", *J. Geophys. Res., 95*, 12681-12685, 1990.

Wood, B. J., The effect of H_2O on the 410-kilometer seismic discontinuity, *Science, 268*, 74-76, 1995.

Yeganeh-Haeri, A., Synthesis and re-investigation of the elastic properties of single-crystal magnesium silicate perovskite, *Phys. Earth Planet. Int., 87*, 111-121, 1994.

Yeganeh-Haeri, A., D. J. Weidner, and E. Ito, Elastic properties of the pyrope-majorite solid solution series, *Geophys. Res. Lett., 17*, 2453-2456, 1990.

L. Stixrude, School of Earth and Atmospheric Sciences, Georgia Institute of Technology, Atlanta, GA 30332-0340. (e-mail: stixrude@perovskite.eas.gatech.edu)

(Received March 1, 1996; revised January 31, 1997; accepted February 19, 1997.)